# Lab on a Chip

Devices and applications at the micro- and nanoscale

## Accepted Manuscript

This article can be cited before page numbers have been issued, to do this please use: V. T. Dau, T. T. Bui, C. Tran., T. V. Nguyen, T. Nguyen, T. Dinh, H. Phan, D. Wibowo, B. Rehm, H. T. Ta, N. Nguyen and D. V. Dao, *Lab Chip*, 2021, DOI: 10.1039/D0LC01247E.

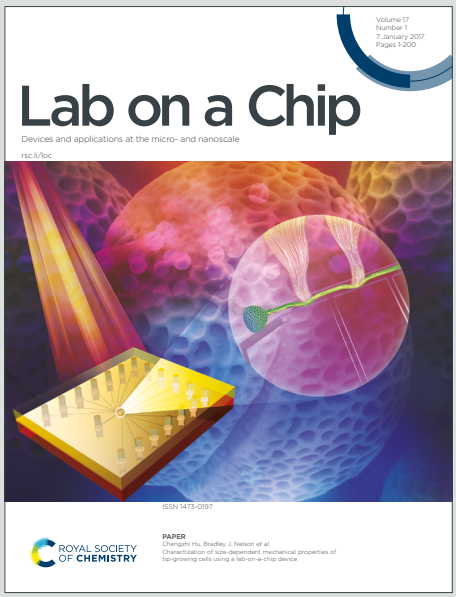

View Article Online
DOI: 10.1039/D0LC01247E



# In-Air Particle Generation by On-Chip Electrohydrodynamics

Van T. Dau[1,7], Tung T. Bui[2], Canh-Dung Tran[3], Thanh Viet Nguyen[4], Tuan-Khoa Nguyen[4], Toan Dinh[3], Hoang-Phuong Phan[4], David Wibowo[5], Bernd H.A. Rehm[5], Hang Thu Ta[4,6], Nam-Trung Nguyen[4] and Dzung V. Dao[1,4]

[1]School of Engineering and Built Environment, Griffith University, AUSTRALIA

[2]University of Engineering and Technology, Vietnam National University, Hanoi, VIETNAM

[3]School of Mechanical and Electrical Engineering, University of Southern Queensland, AUSTRALIA

[4]Queensland Micro and Nanotechnology Centre, Griffith University, AUSTRALIA

[5]Centre for Cell Factories and Biopolymers, Griffith Institute for Drug Discovery, Griffith University, AUSTRALIA

[6]School of Environment and Science, Griffith University, AUSTRALIA

[7]Centre of Catalysis and Clean Energy, Griffith University, AUSTRALIA





***Abstract***

Electrohydrodynamic atomization has been emerging as a powerful approach for respiratory treatment, including the generation and delivery of micro/nanoparticles as carriers for drugs and antigens. In this work, we presents a new conceptual design in which two nozzles facilitate dual electrospray coexisting with ionic wind at chamfered tips by a direct current power source. Experimental results by a prototype have demonstrated the capability of simultaneously generating-and-delivering a stream of charged reduced particles. The concept can be beneficial to pulmonary nano-medicine delivery since the mist of nanoparticles is migrated without any restriction of either the collector or the assistance of external flow, but is pretty simple in designing and manufacturing devices.

## 1. Introduction

There is an increasing interest in the generation of micro-/nano-particles for inhalable drug/antigen delivery [1]. Advances in particle engineering technologies have led to rapid development of the design, synthesis and application of inhalable micro-/nano-particles encapsulating therapeutics or antigens [2]. Hence, particle-based delivery has emerged as a promising alternative to conventional inhalable drug and vaccine delivery [3]. Human pathogens often enter the body through the nose, mouth, trachea and lungs, thus inhaled drug/antigen delivery could be more effective than parenteral delivery as it can directly prevent local infections in the respiratory tract [4]. Moreover, inhaled drugs do not undergo metabolism, providing unique advantages such as a large surface area of the mucous membranes of the respiratory tract and pulmonary epithelium, the thin membranes between pulmonary alveoli and circulation, and high blood flow from and to these specific organs that all lead to high and rapid absorption into the circulation [5], thus allowing smaller

View Article Online
DOI: 10.1039/D0LC01247E


doses to be administered and a better efficacy-to-safety ratio compared to other delivery systems. Therefore, pulmonary drug administrations through inhalation of actives have been developed for either local or systemic delivery, including (i) anti-allergic agents for bronchial asthma [6], (ii) antibiotics for tuberculosis [7] and cystic fibrosis [8] in lungs, (iii) chemotherapeutics for lung cancers [9], (iv) antigens for influenza virus [10] and Bacillus anthracis [11], (v) immunosuppresants for lung transplant rejection prevention [12], (vi) radio contrast agents for imaging of airways [13], and (vii) peptide-loaded nanoparticles for treatment of heart failures [14].

In general, development of micro-/nano-particles for pulmonary drug/antigen delivery involves two consecutive steps: (i) the production of particles loaded with therapeutics or antigens, and (ii) the aerosolization of the particulate therapeutics/vaccine. The deposition of particulate material in respiratory systems is determined by their charges and aerodynamic diameters. Particles with high residual of positive/negative charge or with aerodynamic diameter bigger than 5 μm accumulate preferentially in the upper respiratory tract (mouth, throat) [15–17]. The particles in size ranges 1-5 μm can have maximum depositions corresponding to the size of lower airways. In fact, nanoparticles of less than 0.5 micrometer are exhaled without being deposited [18–21]. A technology that is simple but capable of controlling particle size and charge is ultimately desired, as it allows precise deposition of the particles in specific regions of the lung, thereby improving delivery efficiency, reducing drug exposure to non-targeted regions of the airway, and alleviating any harmful side effects [22].

Several established technologies to generate aerosols for medical application can be cited as pressurised nebuliser, ultrasonic, or piezo-mesh nebuliser. Among them, the piezo-mesh is considered the most efficient one. These technologies still possess some drawbacks such as low accuracy of the delivery rate, high loss of sprayed aerosols and limit droplet size (1.2μm – 20μm) [23]. Several technologies have recently emerged. For example, the colliding jets [24] and extruded jets [25] with medium particle size of 3μm are more effective in delivering inhaled drug candidates than conventional pressurised nebuliser, even with a tiny drug volume of 45 μL. Other approaches are surface acoustic wave [26] and capillary aerosol generator [27] which use vibration to nebulise liquid via acoustic wave and aim for high viscous liquid.

Electrohydrodynamic atomization (EHDA) or electrospray is a superior candidate since the technology can efficiently generate micro/nanoscale droplets and is configurable to even encapsulate complex therapeutic molecules or antigens within a single droplet. This technique has been emerging as a powerful approach for drug discovery research [28,29] and currently attracting interest into respiratory treatment, including the generation and delivery of micro-/nano-particles as carriers for drugs and antigens [30–33].

A typical EHDA system consists of a spray electrode atomizing charged liquid and a reference electrode placed downstream to form an electric field. When liquid in a spray electrode is subjected to a strong electric potential, the accumulated surface charge at the outer interface leads to radial electrostatic pressure deforms the liquid into a conical shape called the Taylor cone. As the charge accumulates, liquid eventually emits into unidirectional jets and breaks into a monodispersed cloud of highly charged particles (positive or negative). In either case, this cloud is driven by electrostatic force, and the majority of particles will land on the reference electrode [34,35].

To directly utilize EHDA for inhalable drug delivery or health care applications, the residual charge of particles must be reduced to weaken the electrostatic force in the inter-electrode space so that the

View Article Online
DOI: 10.1039/D0LC01247E



particles can be conveyed out of the effect of reference electrode. Many efforts have been carried out to address this issue; for instance, mixing the sprayed particle with oppositely charged droplets or oppositely charge gaseous ions or using high-frequency alternating EHDA to stimulate a resonating meniscus at the orifice. Nevertheless, these approaches requires multiple EHDA sources that are actuated independently, or very high frequency (MHz order) to break the meniscus of the liquid, which subsequently require complex driving circuit and limit the practical application of the system [36–42].

We have recently proposed an approach of using low-frequency EHDA to self-neutralize droplet by matching their momentum with the alternating reversed electric field [43]. Here we present another approach, a versatile and novel EHDA system using two spray electrodes which are symmetrically placed from each other and simply powered by a direct current power source. This design concept, named as the bipolar electrostatic atomization (BESA), generates a stream of nanoparticles with very low electrical charge. The experiments show that testing liquids, with and without suspending solid particles, can be steadily sprayed, and the sprayed droplets moves away from both electrodes to reach to a targeted region. Our concept is simple and can be beneficial to pulmonary nano-medicine delivery since the mist of nanoparticles are delivered without the restriction of either the collector or the assistance of external flow.

## 2. Concept and Design

Figure 1 shows our BESA concept using two spray electrodes symmetrically placed and connected with two polarities of a single high-voltage DC source powered by a battery. The mutual inter-electrode electric field generates electrospray at both nozzles. As the system is primarily disconnected from the ground, it yields a charge balance and simultaneous charge neutralization as discussed next. BESA is fundamentally distinguished from conventional multi-electrospray designs, where each electrospray is independently setup. In our new concept, the two nozzles play the role of both spray electrode and reference electrode and define the electric field.

With the new configuration, the electric field will be bent outward the electrode axes. To facilitate this effect, we design chamfered nozzle tips to direct the spray. When a liquid is fed into the nozzle, it will migrate to the chamfered tip due to the Coanda effect and will be sprayed from there. Compare to other tip types such as flat one, the chamfered tip creates a higher electric field strength and a larger effective meniscus radius $r$, i.e. lower capillary pressure, which eases the starting condition for the formation of electrospray from the Taylor cone when the electrostatic pressure surpasses the liquid capillary pressure $\varepsilon_0 E^2/2 > \sigma_s/r$. Therefore, a relevant chamfer cut angle at the nozzle plays a vital role to initially direct the spraying and reduce the initial voltage to start the spraying process.

View Article Online
DOI: 10.1039/D0LC01247E


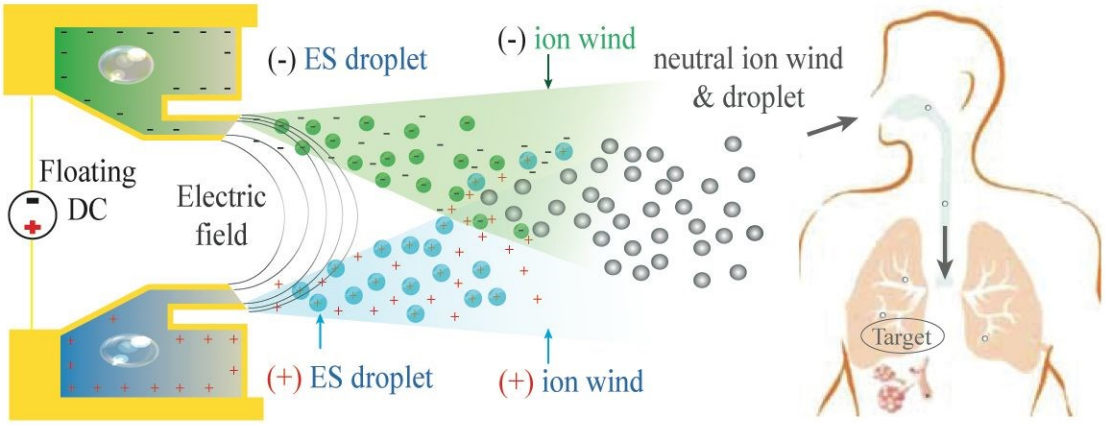


***Figure 1.*** *Principle of the present BESA using symmetrical electrode configuration with electrospray at each electrode. The streamlines represent electric field between chambered nozzle tips.*

Due to the highly concentrated electric field at the chamfered tips, ionization processes in the air surrounding the nozzle can be expected. Therefore, the spray cloud would be composed of both ionic wind and electro-sprayed particles. After being generated at the vicinity of the electrode tips, the two clouds gain initial momentum to move away along the direction parallel with the electrode axes. The electric field controls the two clouds of opposing polarities to impinge each other inside the area between the spray electrodes. The ionic winds, which carry much more residual charge than the electro-sprayed particles, also possess a high recombination rate quickly neutralize the oppositely charged particles and effectively cut-off the amount of net charge. Therefore the electrostatic force acting on this cloud diminishes [44,45]. The cloud of neutralized ions and particles moves forward due to the gained momentum. Thus, the present symmetrical configuration allows the electro-sprayed particles to neutralize each other and move away from the electrodes.

## 3. Electrohydrodynamic simulation

The generation of the liquid cone and jet at the chamfered nozzle tip can be simulated using a computational fluid dynamic model [46]. The liquid meniscus is tracked by a level set function ϕ, where ϕ=1 represents the liquid and ϕ=0 represents the surrounding air. Assuming liquid is linear dielectric and incompressible, the motion of liquid and its meniscus in an electric field is described by the level set equation, continuity equation and momentum conservation equation.

$$\frac{\partial \phi}{\partial t} + \vec{u} \cdot \nabla \phi = \nabla \cdot (\nabla \phi - \phi(1-\phi)) \frac{\nabla \phi}{|\nabla \phi|} \qquad (1)$$

$$\nabla \cdot \vec{u} = 0 \qquad (2)$$

$$\rho\left[\frac{d\vec{u}}{dt} + (\vec{u} \cdot \nabla)\vec{u}\right] = -\nabla p + \eta \nabla^2 \vec{u} + \overrightarrow{\sigma_s} + \overrightarrow{f_e} + \rho \vec{g} \qquad (3)$$

where $p$ is the pressure, $\vec{u}$ is the fluid velocity, $\overrightarrow{\sigma_s}$ the force due to the surface tension and $\vec{g}$ the gravitational constant.

The electrical body force $\overrightarrow{f_e}$ for an incompressible liquid is calculated by taking the divergence of Maxwell stress tensor [47]

$$\overrightarrow{f_e} = q\vec{E} - \frac{1}{2}\varepsilon_0 E^2 \nabla \varepsilon + \nabla\left(\frac{1}{2}\varepsilon_0 E^2 \frac{\partial \varepsilon}{\partial \rho}\rho\right) \quad (4)$$

View Article Online
DOI: 10.1039/D0LC01247E


where $q$ is the charge density, $\varepsilon$ is the relative dielectric constant of the liquid, $\varepsilon_0 =$ 8.85 pF/m is the permittivity of vacuum, and $\vec{E}$ is the electric field. The first term is the free charge force, the second is due to inhomogeneities in the dielectric and the last term results from changes in the material density, which is commonly negligible [48].

The charge density is determined by Gauss's law as

$$q = \varepsilon\varepsilon_0 \nabla \cdot \vec{E} = -\varepsilon\varepsilon_0 \nabla^2 V \qquad (5)$$

with $V$ the electric potential. In addition, the charge conservation is described as

$$-\frac{dq}{dt} = \nabla \cdot \vec{J} = \nabla \cdot \left(q\vec{u} + \sigma\vec{E}\right) \qquad (6)$$

where $\sigma$ is the electrical conductivity of the liquid.

The two-phase numerical simulation consisting of liquid and air is carried out in the COMSOL environment. Since the permittivity of liquid is different from one of surrounding air, the permittivity of each grid cell is calculated using the level set function with $\varepsilon = 1 + \left(\varepsilon_{liquid}/\varepsilon_{air} - 1\right)\phi$. The nozzle tip is chamfered at angle of 60° and applied by a voltage of 2300 V. For the sake of simplicity, the ground electrode is placed normal to the nozzle axis at a distance of 1.5 mm from the tip. A working liquid is dipropyleneglycol monomethyl ether (DPM), its physical properties are surface tension $\sigma_s = 29\ \mathrm{mN/m}$, density $\rho = 0.96\ \mathrm{g/ml}$, viscosity $\mu = 4.5\ \mathrm{mPas}$ and relative permittivity $\varepsilon = 10.5$. The flow rate of the liquid is typically approximated by $Q \sim \sigma_s\varepsilon\varepsilon_0/\rho\sigma$ for stable Taylor cone [49] and is set up at $1\ \mathrm{ml/h}$ into the nozzle.

It is worth noting that DPM is a popular liquid used in cosmetics with low toxicity and polyethylene glycol (PEG) has been recently used to circulate extracellular vesicle-derived DNA [50]. A mixture of DPM and PEG which can be used as solvent for poorly water-soluble drugs [51] thus is applied in our work to demonstrate the reliability and applicability of the device. Several U.S. Food and Drug Administration-approved solvents for drug delivery will be used in our coming further developments.

The simulation result is shown in Fig. 2. As expected, liquid firstly migrates to the tip of the nozzle due to its wettability (Fig2, t=0.0007s). When a sufficient electric field strength acts on the liquid surface, the charge density induced on the surface yields a radial electrostatic pressure which is equilibrium with the surface tension. The sharp cut-tip at the nozzle concentrates the electric field, encourages the natural instability of the meniscus, creating the singularity that is again multiplied by the subsequent concentration of electric field (t=0.015s). The liquid deforms into a conical shape and a jet is generated from the chamfered tip (t=0.025s). The flat tip, as discussed, is less favorable to facilitate singularity and thus requires a higher voltage to overcome capillary pressure.

View Article Online
DOI: 10.1039/D0LC01247E




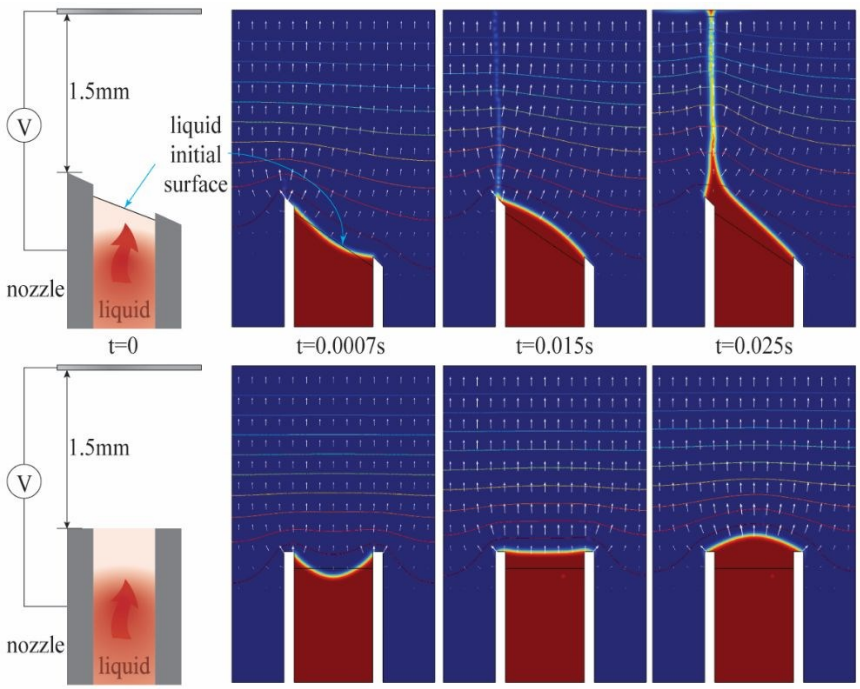


***Figure 2.*** *Transient simulation of the Taylor cone formation for chamfered sharp tip nozzle (top) and flat-tip nozzle (bottom): model (left), and simulation results of liquid meniscus movement, potential distribution (contour lines) and electric field (white arrows) at different times.*

These starting voltages for nozzles of flat tip and chamfered tip are experimentally observed. For this experiment mimicking the configuration in Fig 2, a positive voltage is applied to the nozzle which is standard gauge 27 stainless steel and the working liquid (DPM) is pumped with a range of flow rates from 0.2ml/h – 2ml/h. Experimental results in Fig 3 confirmed that for all testing flowrates, the starting voltage for chamfered tip nozzle is lower and more stable than those of the flat tip nozzle.

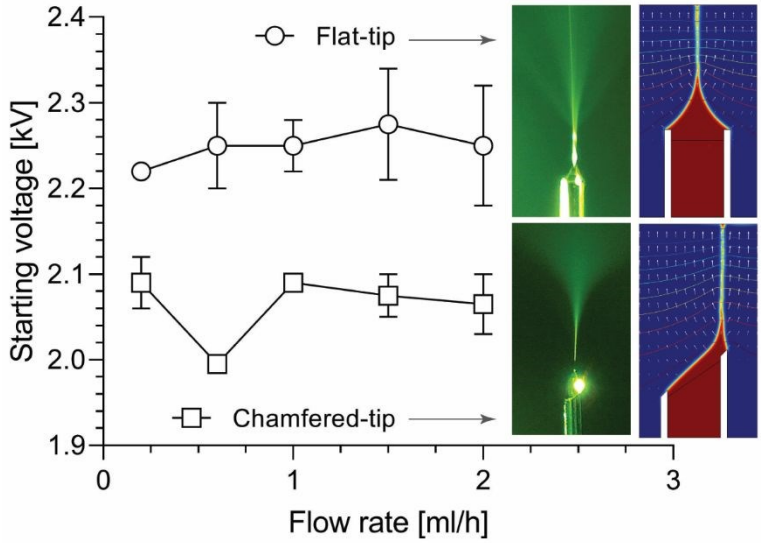


***Figure 3.*** *Measurement of starting voltages for nozzles with flat-tip and chamfered tip in nozzle-plane configuration. The insets show pictures of Taylor cone at nozzle tip and corresponding simulated results. Each experiment was indepentednly repeated three times. Results are shown with SEM error bars.*

View Article Online
DOI: 10.1039/D0LC01247E



The current-voltage (I–V) characteristics of chamfered tip nozzle is measured and shown in Fig. 4, with the inset confirmed that corona discharge starts at the tip of the nozzle and coexist with electrospray. The current continues increasing with the increase of the voltage, which can be used to control the electrospray regime (Figures S1 and S2, supplementary material). It is noted that this corona discharge usually does not disturb the spraying process [52]. Nevertheless, we further limit the discharge current within a few μAs, i.e. a two orders of magnitude smaller than a typical corona discharge, to minimize the unexpected effect such as streamer discharge. In our previous work, we proved that a current of ~2 μA is sufficient to generate strong ionic wind that can manipulate the movement of micro-/nano-particles [53,54].

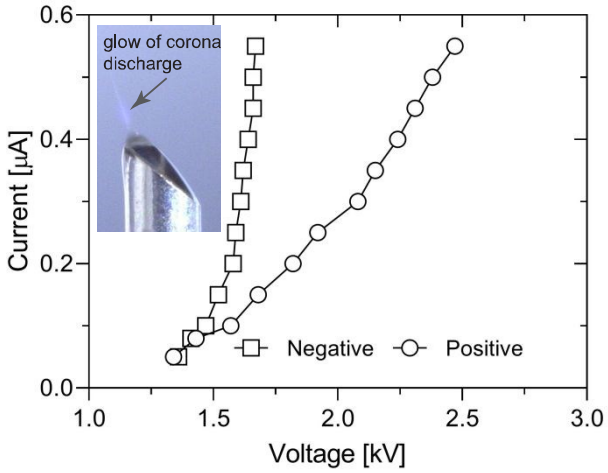


***Figure 4.*** *I-V characteristics of the electrospray from chamfered nozzle is measure for the positive and negative electrosprays to compare the I-V characteristics of the two cases. The negative electrospray has a higher current at a lower voltage due to the lower onset voltage of negative corona.*

## 4. Methodology and Technical Implementation of BESA device

A 10mm x 10mm nozzle device was fabricated by micro-technology. A 400 μm silicon wafer was dry-etched from the top to form two wells as the liquid chambers; each chamber is connected to a nozzle with the same depth of 130 μm. A dry-etching process is used again from the bottom to release the free-standing nozzles. These free-standing structures are important as they promote capillary force that draws liquid from the liquid chamber up to the nozzle tips, while preventing the liquid from further migrating to the substrate. The distance between two nozzles is 2 mm. A thin gold layer is coated on the whole surface of the chip to increase connection between the on-chip and off-chip circuits. The fabricated chip is soldered on a printed circuit board, and the bridge between the two liquid wells are finally removed to release two independent chamber-nozzle sets that are symmetrically positioned. Two nozzles/electrodes are further electrically isolated by conformal coating (Shinetsu Ltd.) which also prevent migration of liquid between chambers (see Fig.5a).

View Article Online
DOI: 10.1039/D0LC01247E


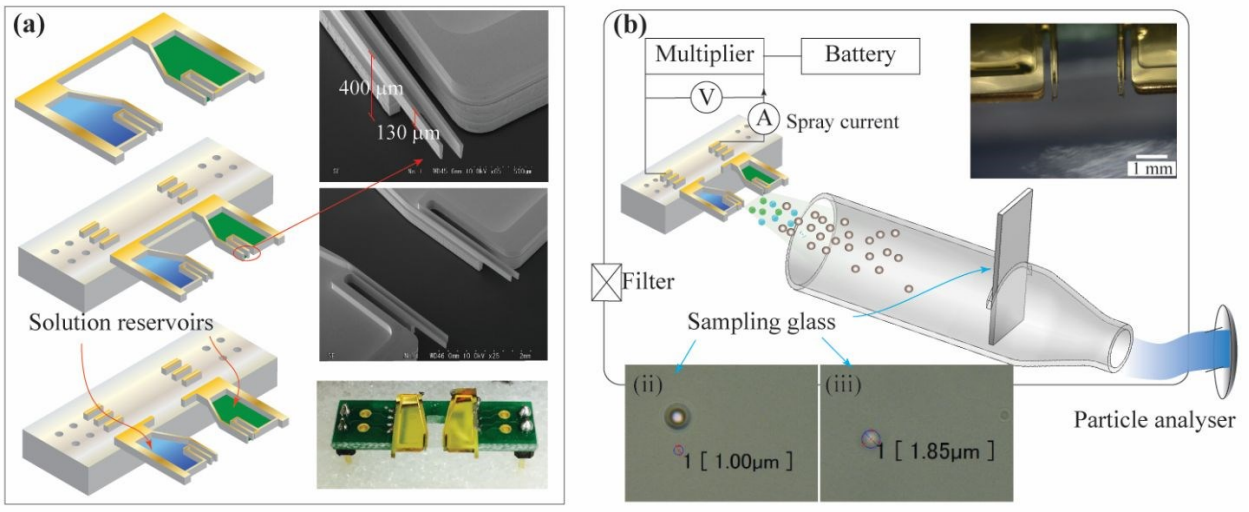


***Figure 5***. *Micro-droplet generation using on-chip BESA of our new approach: (a) a schematic of the system, (b) experiment setup for droplet characterization. The droplets and particles can be observed on sample glass, (i) a zoomed view of sprayed polystyrene particle with white core, (ii) a zoomed view of sprayed droplet. The dimensions of each reservoir are 4mm × 2mm × 0.4mm.*

Two poles of a customized high-voltage generator generating a DC voltage up to 8 kV is connected to each chamber. A closed-loop control system is set up to maintain the desired discharge current sensed at the negative electrode by using an adjustable current unit. The discharge current is recorded at the negative electrode using a shunt-resistor and a built-in comparator. A battery is used as an isolated power source to ensure that the current measured at the negative electrode is the mirror image of the current at the positive electrode.

To observe and evaluate the spraying by the present method, test solution is a mixture of 95% DPM (Sigma-Aldrich 99%) and 5% polyethylene glycol (PEG 200, Sigma-Aldrich). This small portion of PEG200 is to slow down the volatility of the sprayed droplets, making the droplet measurement more reliable. Additionally, to investigate the capability of atomizing liquid with and without solid particles (e.g. liquid with immiscible drug particle), polystyrene particles of 1.0 µm diameter are introduced into the solution, which is then fed into the two liquid wells using micro dispenser. The electrospray process is observed using a digital microscope (Dino-lite EDGETM).

## 5. Spray performance of BESA

Figure 6 shows the I-V characteristics of BESA. We observed at both nozzles the electrosprays consequently started at 1.34 kV and the corresponding spray current is 0.11 µA. This current linearly increases to 0.15 µA with voltage of 1.54 V. Over this onset value, the currents firmly step up when the voltage continues to increase, dramatically jump to 0.97 µA when the voltage reaches 1.56 kV. The jump of electric current indicates that the corona discharge started at the nozzle tip and ionic winds flow through the inter-electrode space. The jump of current also infers that most of the electrical charge is transferred into the ionic winds, not the electrospray itself. Thus the ionic winds easily neutralize the stream of droplet of the opposite charge and efficiently drives the droplets away from both electrodes [55]. We also notice the I-V after the current jump does not fully agree with the relation $V \propto \sqrt{I}$ that has been found for dual ionic wind in our previous work [56,57], indicating the co-existence of ionic wind-electrospray slightly changes this relation. Indeed, the co-existence of ionic wind and electrospray could

View Article Online
DOI: 10.1039/D0LC01247E



improve the stability of the Taylor cone, as the corona discharge consumes excessive charges which otherwise quickly transform the single jet to the multiple jet spray modes.

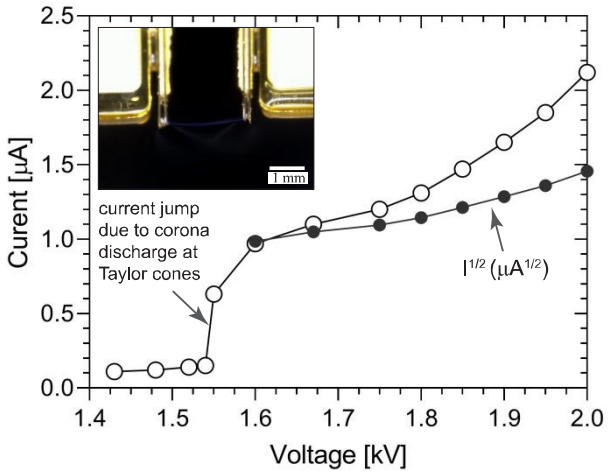


***Figure 6**. I-V Characteristics (I-V) of BESA system: Connecting one nozzle with a positive electrode and another one with the negative electrode of a power source*

BESA device is placed to one side of a plastic tube whose another side is linked to a vacuum pump with a flowrate of 1.0 litre/min (Fig 5b). The solutions with and without suspension polystyrene particles are alternatively fed into BESA liquid chambers and sprayed. The sprayed droplets/particles were collected on a flat glass substrate (Sigma Aldric) located at a distance of 15cm from the device, as shown in Fig. 5b. This glass substrate is pre-covered by deionized water to catch liquid droplets but not to impact their shape. An inversed digital microscope is used to observe the collected particles on the substrate. Experimental observation depicts the appearing of droplets (Fig.5b, inset ii) and polystyrene particles of 1 μm (Fig.5b, inset iii) on the substrate, indicating both liquid and polystyrene particles are atomized and delivered out of the device. A zoom-out picture of substrate capturing droplets is presented in supplementary material (Figure S3).

The distribution of droplet size by BESA was analyzed using an aerosol spectrometer (TSI 3340) which replace the above-mentioned vacuum pump. Experimental observation shown in Fig. 7 indicates a very high aerosol concentration. The droplet distribution has two peaks of ~2 μm and ~0.75 μm, which is close to the lower limit of the used aerosol spectrometer. This measurement also agrees well with the droplet observation on glass substrate in Fig. 5b (insets ii and iii). The aerosol experiment was independently repeated three times with almost identical size distribution of particles. This results demonstrates that charge reduced particles are efficiently generated and delivered, and there is an insignificant difference when spraying solution with and without solid polystyrene particles, Fig. 7b.

View Article Online
DOI: 10.1039/D0LC01247E


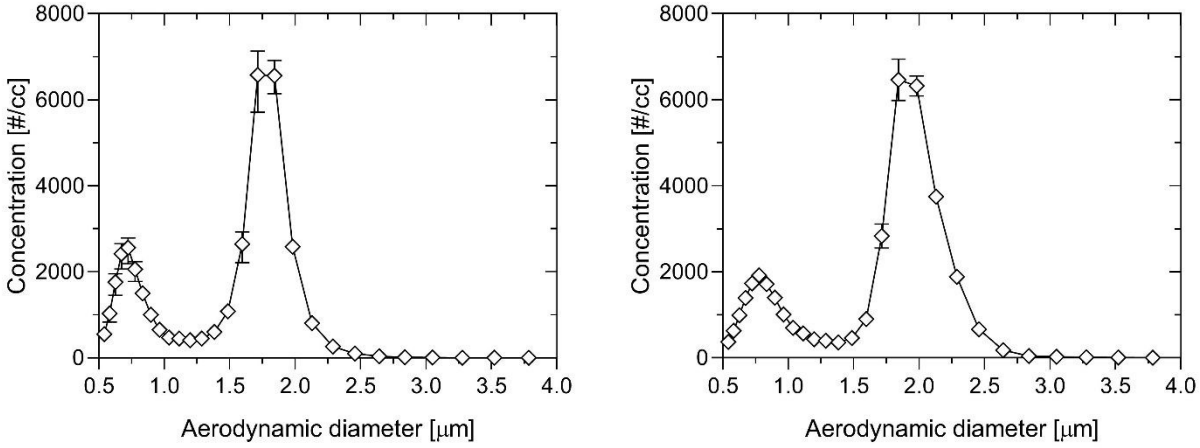


**Figure 7.** *(a, left) Distribution of droplet size at a current of 1μA generated by the present BESA with only liquid solution of PEG and DPM. (b, right) Distribution of droplet size generated by the present BESA at a current of 1μA with polystyrene particle suspended solution of PEG and DPM. Polystyrene particles of 1μm diameter. Each experiment was independently repeated three times.*

There are several ways to control the average aerosol size, such as adjusting the physiochemical properties of liquid, spraying voltage, or the nozzle direction. With a manufactured and installed device (i.e. a given set of parameters of spraying direction and electrode configuration), our experimental results of the present device showed that by alternating the concentration of polyethylene glycol from 0%, 2.5% and 5%, the particles' size increases from ~0.9 μm to ~1.7 μm (Fig.8a).

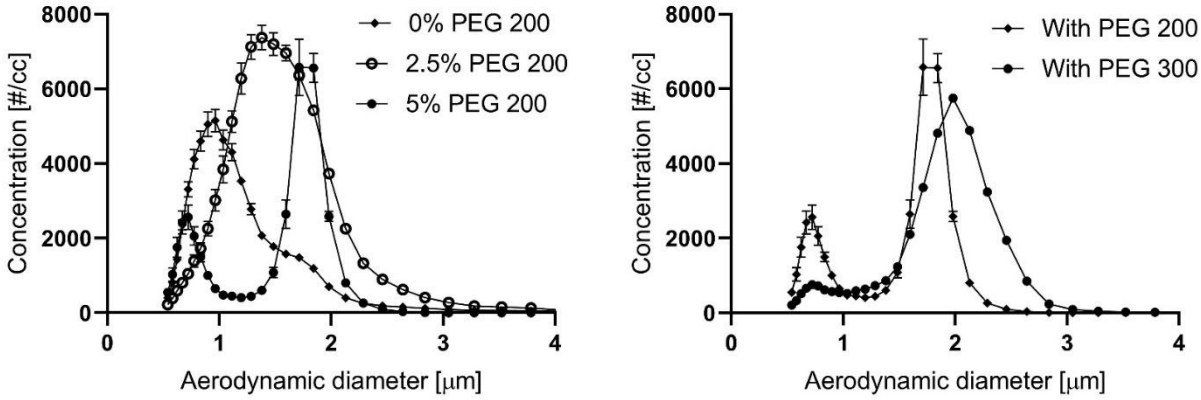


**Figure 8.** *(a, left) Particle size distribution of generated aerosols versus the concentration by the present approach with different concentrations of PEG200. (b, right) Particle size distribution of generated aerosols versus the concentration by the present approach with different type of PEG (PEG 200 and PEG 300)*

Similarly, by changing the type of polyethylene glycol from PEG-200 (average molecular mass 190-210, Sigma Aldrich) to PEG 300 (average molecular mass 285-315, Sigma Aldrich), the particle size increases from ~1.7 μm to ~2.0 μm (Fig. 8b).

For airway deposition, the aerosols should be spherical, uniform in size and uncharged [58]. Two size ranges leading to maximum airway deposition include 50 - 100 nm corresponding to the alveoli and 1 – 5 μm for the lower airways [59]. Most aerosols used in inhalation delivery are for the latter range. The

View Article Online
DOI: 10.1039/D0LC01247E



optimal particle size is estimated at 1-3 µm, with some other studies stated that the optimum size is from 1.4 to 1.8µm. The particles bigger than 5 µm in diameter are usually ingested or deposited in the oropharyngeal region [19–21]. Thus, controlling the particle size is essential to deposit particles into specific regions within the lung, thereby improving delivery efficiency, reducing drug exposure to non-targeted regions of the airway, and alleviating any harmful side effects [22]. The present device can generate aerosols of typical size of around 1.7 µm, which would be suitable for pulmonary drug delivery.

Finally, the charge density of the sprayed droplet by BESA is investigated by an electrometer probe (3608 TSI) installed at the outlet of the test tube. Results by Fig. 9 depict the average charge density of the stream of droplets/particles is approximately 250 fA for both cases solutions with and without polystyrene particles. This extremely low net charge is close to the electrostatic noise in the air and is insignificantly compared with the discharge current at the order of µAs as shown in Fig. 6. In other words, owing to the balance/elimination of the positive and negative charged particles, the device can generate and deliver particles with significantly reduced charges.

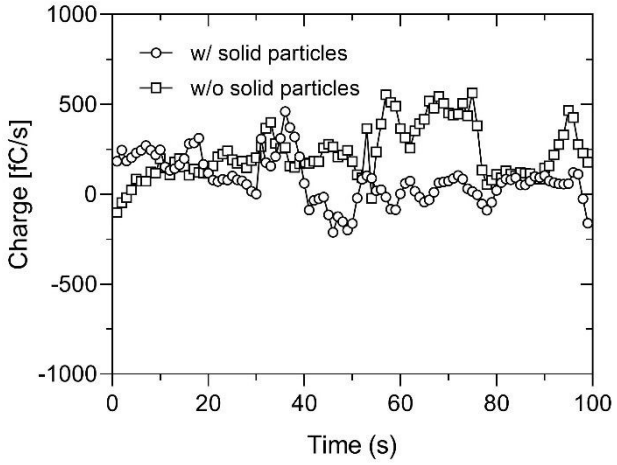


***Figure 9.*** *The charge of droplets by BESA device, measured using an electrometer for two cases (1) solution of PEG/DPM; and (2) polystyrene suspended solution of PED/DPM.*

## 6. Conclusion

We present a new conceptual design of electrospray together with its prototype to demonstrate the capability of simultaneous generate-and-deliver a stream of charged reduced micro/nano-particles. The two nozzles facilitate dual electrospray that coexists with ionic wind at chamfered sharp tips eliminates the need for collector electrode, which is essential in most existing EHDA system. This unique advantage would enable spaying viable droplets in micro/nano-encapsulation, bio-scaffold production as well as polymeric micro/nanoparticle fabrication. The simple design and initial results by experiments enable practical developments for drug delivery and nano-medicine applications where the generation of charge reduced nanoparticle is imperative.

**Author contribution: Van T. Dau**: Conceptualization, Investigation, Formal analysis, Writing - original draft, Methodology, Project administration. **Tung T. Bui**: Conceptualization, Investigation, Data curation, Writing - original draft. **Canh-Dung Tran**: Methodology, Supervision, Writing - review & editing. **Tuan-Khoa Nguyen**: Data curation,

View Article Online
DOI: 10.1039/D0LC01247E


review & editing. **Toan Dinh**: Investigation, review & editing. **Hoang-Phuong Phan**: Writing - review & editing. **David Wibowo**: Methodology, review & editing. **Bernd H.A. Rehm**: Supervision – review & editing. **Hang Thu Ta**: Supervision, Writing - review & editing. **Nam-Trung Nguyen**: Supervision, Writing - review & editing **Dzung Viet Dao**: Supervision, Writing - review & editing, Project administration, Funding acquisition.

## References

[1] J.C. Sung, B.L. Pulliam, D.A. Edwards, Nanoparticles for drug delivery to the lungs, Trends Biotechnol. 25 (2007) 563–570. https://doi.org/10.1016/j.tibtech.2007.09.005.

[2] B.H.A. Rehm, Bioengineering towards self-assembly of particulate vaccines, Curr. Opin. Biotechnol. 48 (2017) 42–53. https://doi.org/10.1016/j.copbio.2017.03.018.

[3] I.M. El-Sherbiny, N.M. El-Baz, M.H. Yacoub, Inhaled nano- and microparticles for drug delivery, Glob. Cardiol. Sci. Pract. 2015 (2015) 2. https://doi.org/10.5339/gcsp.2015.2.

[4] J. Wallis, D.P. Shenton, R.C. Carlisle, Novel approaches for the design, delivery and administration of vaccine technologies, Clin. Exp. Immunol. 196 (2019) 189–204. https://doi.org/10.1111/cei.13287.

[5] J.S. Patton, P.R. Byron, Inhaling medicines : delivering drugs to the body through the lungs, 6 (2007) 67–74. https://doi.org/10.1038/nrd2153.

[6] S. Onoue, Y. Aoki, Y. Kawabata, T. Matsui, K. Yamamoto, H. Sato, Y. Yamauchi, S. Yamada, Development of Inhalable Nanocrystalline Solid Dispersion of Tranilast for Airway Inflammatory Diseases, J. Pharm. Sci. 100 (2011) 622–633.

[7] A. Misra, A.J. Hickey, C. Rossi, G. Borchard, H. Terada, K. Makino, P.B. Fourie, P. Colombo, Inhaled drug therapy for treatment of tuberculosis, Tuberculosis. 91 (2011) 71–81.

[8] C. Velino, F. Carella, A. Adamiano, M. Sanguinetti, A. Vitali, D. Catalucci, F. Bugli, M. Iafisco, Nanomedicine Approaches for the Pulmonary Treatment of Cystic Fibrosis, Front. Bioeng. Biotechnol. 7 (2019) 406.

[9] R. Rosière, T. Berghmans, P. de Vuyst, K. Amighi, N. Wauthoz, The position of inhaled chemotherapy in the care of patients with lung tumors: Clinical feasibility and indications according to recent pharmaceutical progresses, Cancers (Basel). 11 (2019). https://doi.org/10.3390/cancers11030329.

[10] S. Dehghan, M.T. Kheiri, M. Tabatabaiean, S. Darzi, M. Tafaghodi, Dry-powder form of chitosan nanospheres containing influenza virus and adjuvants for nasal immunization, Arch. Pharm. Res. 36 (2013) 981–992.

[11] S.H. Wang, S.M. Kirwan, S.N. Abraham, H.F. Staats, A.J. Hickey, Stable Dry Powder Formulation for Nasal Delivery of Anthrax Vaccine, J. Pharm. Sci. 101 (2012) 31–47.

[12] A. Van Herck, S.E. Verleden, B.M. Vanaudenaerde, G.M. Verleden, R. Vos, Prevention of chronic rejection after lung transplantation, J. Thorac. Dis. 9 (2017) 5472–5488.

[13] N. El-Gendy, K.L. Aillon, C. Berkland, Dry powdered aerosols of diatrizoic acid nanoparticle agglomerates as a lung contrast agent, Int. J. Pharm. 391 (2010) 305–312.

[14] M. Miragoli, P. Ceriotti, M. Iafisco, M. Vacchiano, N. Salvarani, A. Alogna, P. Carullo, G.B. Ramirez-Rodríguez, T. Patrício, L.D. Esposti, F. Rossi, F. Ravanetti, S. Pinelli, R. Alinovi, M. Erreni, S. Rossi, G. Condorelli, H. Post, A. Tampieri, D. Catalucci, Inhalation of peptide-loaded nanoparticles improves heart failure, Sci. Transl. Med. 10 (2018) eaan6205. https://doi.org/10.1126/scitranslmed.aan6205.

[15] O.B. Garbuzenko, G. Mainelis, O. Taratula, T. Minko, Inhalation treatment of lung cancer: the influence of composition, size and shape of nanocarriers on their lung accumulation and retention, Cancer Biol. Med. 11 (2014) 44–55. https://doi.org/10.7497/j.issn.2095-3941.2014.01.004.

[16] T.C. Carvalho, J.I. Peters, R.O. Williams III, Influence of particle size on regional lung deposition – What evidence is there?, Int. J. Pharm. 406 (2011) 1–10. https://doi.org/10.1016/j.ijpharm.2010.12.040.

[17] F. Gagnadoux, J. Hureaux, L. Vecellio, T. Urban, A. Le Pape, I. Valo, J. Montharu, V. Leblond, M. Boisdron-Celle, S. Lerondel, C. Majoral, P. Diot, J.L. Racineux, E. Lemarie, Aerosolized chemotherapy., J. Aerosol Med. Pulm. Drug Deliv. 21 (2008) 61–70. https://doi.org/10.1089/jamp.2007.0656.

[18] P.J. Thompson, Drug delivery to the small airways, Am. J. Respir. Crit. Care Med. 157 (1998) 10–13. https://doi.org/10.1164/ajrccm.157.5.rsaa-7.

[19] P.G.A. Rogueda, D. Traini, The nanoscale in pulmonary delivery. Part 1: Deposition, fate, toxicology and effects, Expert Opin. Drug Deliv. 4 (2007) 595–606. https://doi.org/10.1517/17425247.4.6.595.

[20] P. Zanen, L.T. Go, J.W.J. Lammers, Optimal particle size for β2 agonist and anticholinergic aerosols in patients with severe airflow obstruction, Thorax. 51 (1996) 977–980. https://doi.org/10.1136/thx.51.10.977.

View Article Online
DOI: 10.1039/D0LC01247E





[21] S.P. Newman, M.A. Johnson, S.W. Clarke, Effect of particle size of bronchodilator aerosols on lung distribution and pulmonary function in patients with chronic asthma., Thorax. 43 (1988) 159. https://doi.org/10.1136/thx.43.2.159.

[22] B.Y. Shekunov, P. Chattopadhyay, H.H.Y. Tong, A.H.L. Chow, Particle size analysis in pharmaceutics: Principles, methods and applications, Pharm. Res. 24 (2007) 203–227. https://doi.org/10.1007/s11095-006-9146-7.

[23] T.C. Carvalho, J.T. Mcconville, The function and performance of aqueous aerosol devices for inhalation therapy, J. Pharm. Pharmacol. 68 (2016) 556–578. https://doi.org/10.1111/jphp.12541.

[24] P. Worth Longest, M. Hindle, Evaluation of the respimat soft mist inhaler using a concurrent cfd and in vitro approach, J. Aerosol Med. Pulm. Drug Deliv. 22 (2009) 99–112. https://doi.org/10.1089/jamp.2008.0708.

[25] D. Geller, J. Thipphawong, B. Otulana, D. Caplan, D. Ericson, L. Milgram, J. Okikawa, J. Quan, C. Michael Bowman, Bolus Inhalation of rhDNase with the AERx System in Subjects with Cystic Fibrosis, 2003. www.liebertpub.com (accessed February 10, 2021).

[26] J. Friend, L.Y. Yeo, Microscale acoustofluidics: Microfluidics driven via acoustics and ultrasonics, Rev. Mod. Phys. 83 (2011) 647–704. https://doi.org/10.1103/RevModPhys.83.647.

[27] X. Li, F.E. Blondino, M. Hindle, W.H. Soine, P.R. Byron, Stability and characterization of perphenazine aerosols generated using the capillary aerosol generator, Int. J. Pharm. 303 (2005) 113–124. https://doi.org/10.1016/j.ijpharm.2005.07.010.

[28] S.A. Hofstadler, K.A. Sannes-Lowery, Applications of ESI-MS in drug discovery: interrogation of noncovalent complexes, Nat. Rev. Drug Discov. 5 (2006) 585–595. https://doi.org/10.1038/nrd2083.

[29] M. Wleklinski, B.P. Loren, C.R. Ferreira, Z. Jaman, L. Avramova, T.J.P. Sobreira, D.H. Thompson, R.G. Cooks, High throughput reaction screening using desorption electrospray ionization mass spectrometry, Chem. Sci. 9 (2018) 1647–1653. https://doi.org/10.1039/C7SC04606E.

[30] M. Nikolaou, C.T. Krasia, Electrohydrodynamic methods for the development of pulmonary drug delivery systems, Eur. J. Pharm. Sci. 113 (2018) 29–40.

[31] Q.T. Zhou, P. Tang, S.S.Y. Leung, J.G.Y. Chan, H.K. Chan, Emerging inhalation aerosol devices and strategies: Where are we headed?, Adv. Drug Deliv. Rev. 75 (2014) 3–17. https://doi.org/10.1016/j.addr.2014.03.006.

[32] M.B. Dolovich, R. Dhand, Aerosol drug delivery: Developments in device design and clinical use, Lancet. 377 (2011) 1032–1045. https://doi.org/10.1016/S0140-6736(10)60926-9.

[33] J.-W. Yoo, D.J. Irvine, D.E. Discher, S. Mitragotr, Bio-inspired, bioengineered and biomimetic drug delivery carriers, Nat. Rev. Drug Discov. 10 (2011) 521–535.

[34] A. Jaworek, A.T. Sobczyk, A. Krupa, Electrospray application to powder production and surface coating, J. Aerosol Sci. 125 (2018) 57–92. https://doi.org/10.1016/j.jaerosci.2018.04.006.

[35] G.M.H. Meesters, P.H.W. Vercoulen, J.C.M. Marijnissen, B. Scarlett, Generation of micron-sized droplets from the Taylor cone, J. Aerosol Sci. 23 (1992) 37–49. https://doi.org/10.1016/0021-8502(92)90316-N.

[36] J. Fernandez de la Mora, C. Barrios-Collado, A bipolar electrospray source of singly charged salt clusters of precisely controlled composition, Aerosol Sci. Technol. 51 (2017) 778–786. https://doi.org/10.1080/02786826.2017.1302070.

[37] J.P. Borra, D. Camelot, K.L. Chou, P.J. Kooyman, J.C.M. Marijnissen, B. Scarlett, Bipolar coagulation for powder production: Micro-mixing inside droplets, J. Aerosol Sci. 30 (1999) 945–958. https://doi.org/10.1016/S0021-8502(98)00757-5.

[38] J.P. Borra, D. Camelot, J.C.M. Marijnissen, B. Scarlett, A new production process of powders with defined properties by electrohydrodynamic atomization of liquids and post-production electrical mixing, J. Electrostat. 40–41 (1997) 633–638. https://doi.org/10.1016/S0304-3886(97)00065-X.

[39] V.T. Dau, T. Terebessy, Electrostatic spraying apparatus, and current control method for electrostatic spraying apparatus, US patent No. US9937508, 2014.

[40] L.Y. Yeo, D. Lastochkin, S.C. Wang, H.C. Chang, A new ac electrospray mechanism by Maxwell-Wagner polarization and capillary resonance, Phys. Rev. Lett. 92 (2004) 2–5. https://doi.org/10.1103/PhysRevLett.92.133902.

[41] P. Wang, S. Maheshwari, H.C. Chang, Polyhedra formation and transient cone ejection of a resonant microdrop forced by an ac electric field, Phys. Rev. Lett. 96 (2006) 3–6. https://doi.org/10.1103/PhysRevLett.96.254502.

[42] D.B. Bober, C.-H. Chen, Pulsating electrohydrodynamic cone-jets: from choked jet to oscillating cone, J. Fluid Mech. 689 (2011) 552–563. https://doi.org/10.1017/jfm.2011.453.

[43] V.T. Dau, T.-K. Nguyen, D.V. Dao, Charge reduced nanoparticles by sub-kHz ac electrohydrodynamic atomization toward drug delivery applications, Appl. Phys. Lett. 116 (2020) 023703.

View Article Online
DOI: 10.1039/D0LC01247E


https://doi.org/10.1063/1.5133714.
[44] B.M. Smirnov, H.S.W.M. Sir., Negative ions, 1982.
[45] V.T. Dau, T.X. Dinh, T.T. Bui, C.D. Tran, H.T. Phan, T. Terebessy, Corona based air-flow using parallel discharge electrodes, Exp. Therm. Fluid Sci. 79 (2016) 52–56. https://doi.org/10.1016/j.expthermflusci.2016.06.023.
[46] W. Du, S. Chaudhuri, A multiphysics model for charged liquid droplet breakup in electric fields, Int. J. Multiph. Flow. 90 (2017) 46–56. https://doi.org/10.1016/j.ijmultiphaseflow.2016.11.009.
[47] Herbert H.Woodson, J.R. Melcher, Field description of magnetic and electric forces, in: Electromechanical Dyn., John Wiley & Sons, 1968: pp. 418–466.
[48] A.M. Gañán-Calvo, J.M. López-Herrera, M.A. Herrada, A. Ramos, J.M. Montanero, Review on the physics of electrospray: From electrokinetics to the operating conditions of single and coaxial Taylor cone-jets, and AC electrospray, J. Aerosol Sci. (2018) 1–25. https://doi.org/10.1016/j.jaerosci.2018.05.002.
[49] A.M. Gañán-Calvo, J.M. López-Herrera, N. Rebollo-Muñoz, J.M. Montanero, The onset of electrospray: the universal scaling laws of the first ejection, Sci. Rep. 6 (2016) 32357. https://doi.org/10.1038/srep32357.
[50] N. García-Romero, R. Madurga, G. Rackov, I. Palacín-Aliana, R. Núñez-Torres, A. Asensi-Puig, J. Carrión-Navarro, S. Esteban-Rubio, H. Peinado, A. González-Neira, V. González-Rumayor, C. Belda-Iniesta, A. Ayuso-Sacido, Polyethylene glycol improves current methods for circulating extracellular vesicle-derived DNA isolation, J. Transl. Med. 17 (2019) 75. https://doi.org/10.1186/s12967-019-1825-3.
[51] E.-S. Ha, S.-K. Lee, D.H. Choi, S.H. Jeong, S.-J. Hwang, M.-S. Kim, Application of diethylene glycol monoethyl ether in solubilization of poorly water-soluble drugs, J. Pharm. Investig. 50 (2020) 231–250. https://doi.org/10.1007/s40005-019-00454-y.
[52] A. Jaworek, T. Czech, E. Rajch, M. Lackowski, Spectroscopic studies of electric discharges in electrospraying, J. Electrostat. 63 (2005) 635–641. https://doi.org/10.1016/j.elstat.2005.03.029.
[53] V.T. Dau, T.X. Dinh, C.-D. Tran, T. Terebessy, T.C. Duc, T.T. Bui, Particle precipitation by bipolar corona discharge ion winds, J. Aerosol Sci. 124 (2018) 83–94. https://doi.org/10.1016/j.jaerosci.2018.07.007.
[54] V.T. Dau, T.X. Dinh, T. Terebessy, T.T. Bui, Ion Wind Generator Utilizing Bipolar Discharge in Parallel Pin Geometry, IEEE Trans. Plasma Sci. 44 (2016) 2979–2987. https://doi.org/10.1109/TPS.2016.2580574.
[55] V.T. Dau, T.X. Dinh, T. Terebessy, T.T. Bui, Bipolar corona discharge based air flow generation with low net charge, Sensors Actuators A Phys. 244 (2016) 146–155. https://doi.org/10.1016/j.sna.2016.03.028.
[56] V.T. Dau, C.D. Tran, T.X. Dinh, L.B. Dang, T. Terebessy, T.T. Bui, Estimating the effect of asymmetric electrodes in bipolar discharge ion wind generator, IEEE Trans. Dielectr. Electr. Insul. 25 (2018) 900–907. https://doi.org/10.1109/TDEI.2018.006881.
[57] V.T. Dau, T.X. Dinh, T.T. Bui, T. Terebessy, Bipolar corona assisted jet flow for fluidic application, Flow Meas. Instrum. 50 (2016) 252–260. https://doi.org/10.1016/j.flowmeasinst.2016.07.005.
[58] M.R.C. Marques, Q. Choo, M. Ashtikar, T.C. Rocha, S. Bremer-Hoffmann, M.G. Wacker, Nanomedicines - Tiny particles and big challenges, Adv. Drug Deliv. Rev. 151–152 (2019) 23–43. https://doi.org/10.1016/j.addr.2019.06.003.
[59] G. Ferron, Aerosol properties and lung deposition, Eur. Respir. J. 7 (1994) 1392–1394. https://doi.org/10.1183/09031936.94.07081392.

Electronic Supplementary Material (ESI) for Lab on a Chip.


# In-Air Particle Generation by On-Chip Electrohydrodynamics

(Supplementary Material)

Three spraying modes are observed under different ranges of applied voltage on the nozzle, which are typically called as dripping mode, single jet mode and multiple jet mode. In the single-jet mode, the applied voltage is strong enough to establish a stable electrospray with the visible Taylor cone. As applied voltage continues to increase, the stronger electric field causes the spray to disperse unstably. Once the voltage reaches a specific value, the spray enters multiple jet mode in which the spray breaks into multiple and stable jets, the number of jets increases with the applied voltage.

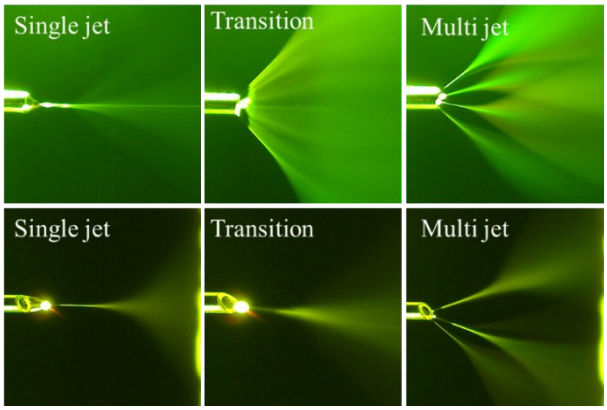


Figure S1. Spray mode of flat-tip and chamfered tip nozzles

The required voltage to overcome dripping mode does not significantly depend on the flow rates. Notably, the stable single jet mode can be established within a wide range of voltage for the chamfered nozzle. There are two reasons for this phenomenon; firstly, the chamfered nozzle allows the single jet to create an angle against the horizontal line before completely transforming into multiple jet mode, secondly, the chamfered nozzle encourage corona discharge that turns excessive charge into ionic wind and stabilises the spray process.

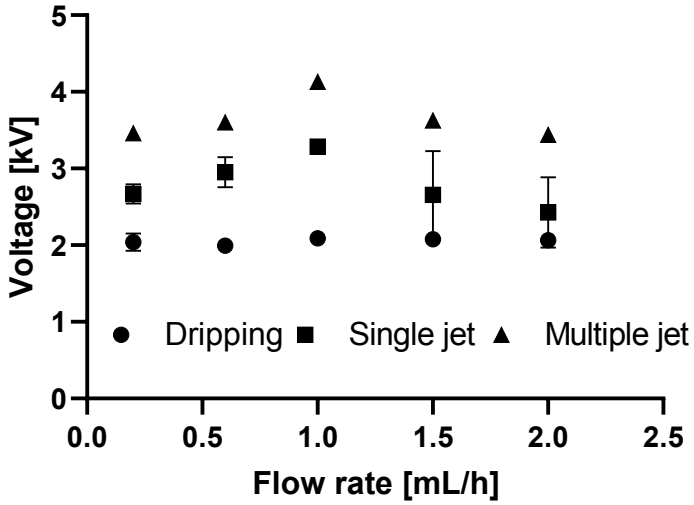


Figure S2. Voltage thresholds for spray mode at different flow rates

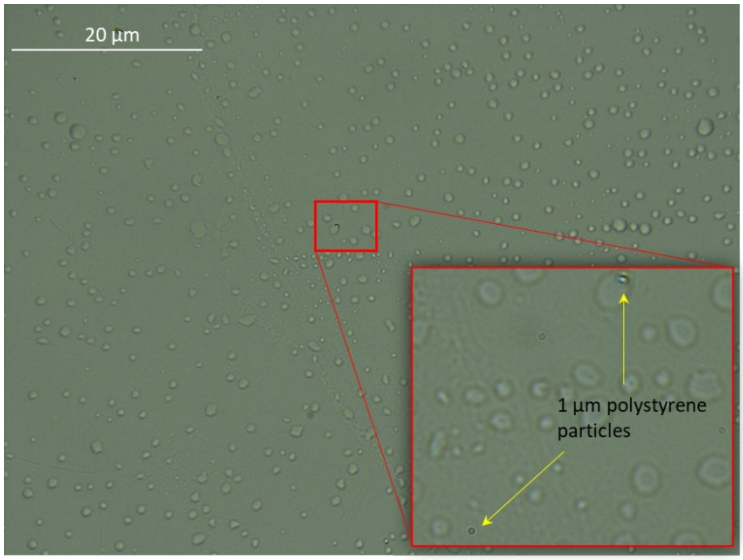


Figure S3. Deposition of sprayed droplets/particles on the glass substrate